

Observational Consequences of Evolution of Primordial Fluctuations in Scalar-Tensor Cosmology

Ryo Nagata,^{1,2,*} Takeshi Chiba,² and Naoshi Sugiyama^{1,†}

¹*Division of Theoretical Astrophysics, National Astronomical Observatory, 2-21-1, Osawa, Mitaka, Tokyo 181-8588, Japan*

²*Department of Physics, Kyoto University, Kyoto 606-8502, Japan*

(Dated: October 27, 2018)

Evolution of primordial fluctuations in a Brans-Dicke type scalar-tensor gravity theory is comprehensively investigated. The harmonic attractor model, in which the scalar field has its harmonic effective potential in the Einstein conformal frame and the theory relaxes toward Einstein gravity with time, is considered. The evolution of adiabatic initial perturbations in flat Λ CDM models is examined from the radiation-dominated epoch up to the present. We discuss how the scalar-tensor gravity affects the evolution of metric and matter perturbations, mainly focusing on the observational consequences, i.e., the matter power spectrum and the power spectrum of cosmic microwave background temperature. We find that the early time deviation is characterized only by the large static gravitational constant while the late time behavior is qualitatively different from that in Einstein gravity because the time variation of the gravitational constant and its fluctuation have non-negligible effects. The attracting scalar-tensor gravity affects only small scale modes due to its attracting nature, the degree of which is far beyond the post-Newtonian deviation at the present epoch.

PACS numbers: 98.65.Dx ; 98.80.Es ; 04.80.Cc

I. INTRODUCTION

The existence of massless scalar partners associated with the tensor field of Einstein gravity is generically predicted by the recent attempts toward unifying all elementary forces in nature based on supergravity, superstrings [1], and other higher dimensional gravity theories. In these theories, time variations of fundamental constants such as the gravitational constant and the fine structure constant are naturally introduced. A recent claim of the time varying fine structure constant from observations of QSO absorption lines [2] may be a piece of evidence.

Scalar-tensor gravity theories, whose original version was proposed by Jordan [3] and Brans and Dicke [4] and were extended in a more general framework later [5], naturally provide coupling between the massless scalar fields and the tensor field of Einstein gravity. Scalar-tensor gravity theories are almost only possible alternatives to Einstein gravity. Moreover, scalar-tensor theories may supply a new approach to implementing the inflationary scenario (called extended inflation) [6]-[9]. The time-varying gravitational “constant” which is their distinctive feature slows the inflationary expansion from exponential to power-law in time, and then the inflationary epoch has finite period, thereby solving the so-called “graceful exit” problem. Furthermore, scalar-tensor theories provide a natural framework of realizing the time-variation of fundamental constants (gravitational constant) via the

dynamics of the Brans-Dicke dilaton (for review see [10]).

In the Jordan-Brans-Dicke theory [3],[4] (hereafter, we refer to it as the Brans-Dicke theory for simplicity) which is the simplest example of scalar-tensor theories, a constant parameter ω is introduced. In the limit $\omega \rightarrow \infty$, the gravitational constant can not change and Einstein gravity is recovered. Although scalar-tensor theories including the Brans-Dicke theory are compatible with Einstein gravity in several aspects, they have many deviations from it. Weak-field experimental tests in solar-system have constrained the post-Newtonian deviation from Einstein gravity, $\omega > 500$ [11],[12]. Measurement of the signal time delay of millisecond pulsars or the light deflection of quasars may raise this limit [13].

In more general scalar-tensor theories, ω can vary depending on the scalar field. In cosmological models based on such theories, it has been pointed out that there is generally an attractor mechanism that drives ω to ∞ in the late cosmological epochs [14]. The nature of gravity can be significantly different in the early universe. Hence, information on the different cosmological epochs may constrain such theories. A simple and natural extension of the Brans-Dicke theory to the attractor model is the harmonic attractor model in which the scalar field has a quadratic effective potential of a positive curvature in the Einstein conformal frame. The analysis of big-bang nucleosynthesis (BBN) in this model [15] restricts two parameters characterizing the potential (its curvature β and today’s gradient α_0). It is concluded that the BBN limit on the possible deviation from Einstein gravity ($2\omega_0 + 3 = \alpha_0^{-2}$) is much stronger than the present observational limits in large $\beta (> 0.3)$ models. Aside from BBN, we have another source of the information about the early universe that is the cosmic

*Electronic address: nagata@th.nao.ac.jp

†Also at Max Planck Institute for Astrophysics, Karl-Schwarzschild-Str. 1 Postfach 1317 D-85741 Garching, Germany

microwave background (CMB). The trace of primordial fluctuation can be seen clearly in the CMB anisotropy spectrum where the information on the early universe up to the last scattering time ($z \sim 1000$) is integrated on the acoustic peaks. The precise CMB data which will be provided in near future [16],[17] should further constrain the allowed parameter region. Toward probing gravity theories by CMB data, we examine the cosmological perturbation evolution in the context of scalar-tensor gravity theories.

Our primary goal is to clarify the growth process of perturbations in the scalar-tensor cosmology and understand the influence on the resultant observable power spectra. We also revisit the perturbations of the Brans-Dicke theory which has been investigated by several authors [18, 19, 20]. Although the contemporary plausible model is a vacuum dominated model, we adopt flat standard CDM (SCDM) models for three reasons. The first reason is that the universe necessarily experiences matter domination once at least. Therefore, we should begin by revealing the effect of the scalar-tensor gravity up to the matter-dominated epoch without confusing curvature or vacuum energy effect with it. The second reason is that the dependence of the scalar evolution on the matter density ($\Omega_0 h^2$) is quite simple as shown in Section IV. The final reason is that, if we take account of the current constraint for ω_0 , the attracting scalar-tensor gravity virtually becomes Einstein gravity before vacuum domination and hence any extra process originating from the scalar-tensor gravity would not occur after vacuum domination.

This paper is organized as follows: In Section II, the field equations and the background cosmological evolution equations in the scalar-tensor theory are described. In Section III, we present the cosmological perturbation theory based on the scalar-tensor gravity. We demonstrate the numerical calculations in Section IV. The resultant matter power spectra and the CMB temperature anisotropy spectra are illustrated in Section V. Finally, some conclusions are in Section VI. In Appendix, the analytic approximate solutions of the background and the perturbation equations in the Brans-Dicke theory are discussed.

II. MODEL

In this section, we describe the scalar-tensor theory and the (unperturbed) cosmological model based on it. We do not assume a specific form of $\omega(\phi)$ as a function of the scalar field ϕ until performing numerical calculations.

A. Field equation

The action describing a general massless tensor-monomonosc scalar theory is

$$S = \frac{1}{16\pi} \int d^4x \sqrt{-g} \left[\phi R - \frac{\omega(\phi)}{\phi} (\nabla\phi)^2 \right] + S_m[\psi, g_{\mu\nu}], \quad (1)$$

where $R = g^{\mu\nu} R_{\mu\nu}$ denotes the scalar curvature of the metric $g_{\mu\nu}$. The last term in Eq.(1) denotes the action of the matter which is a functional of the matter variable ψ and the metric $g_{\mu\nu}$. $\omega(\phi)$ is a function of ϕ and it works as the coupling parameter of the nonminimal coupling. We redefine the scalar field so that it is dimensionless

$$\phi \rightarrow \frac{\phi}{G}, \quad (2)$$

where G is the Newtonian gravitational constant measured today. The field equations are

$$R_{\mu\nu} - \frac{1}{2} g_{\mu\nu} R = \frac{8\pi G}{\phi} T_{\mu\nu} + \frac{1}{\phi} (\nabla_\mu \nabla_\nu \phi - g_{\mu\nu} \square\phi) + \frac{\omega}{\phi^2} \left\{ \nabla_\mu \phi \nabla_\nu \phi - \frac{1}{2} g_{\mu\nu} (\nabla\phi)^2 \right\} \quad (3)$$

and

$$R + 2\frac{\omega}{\phi} \square\phi = -\left(\frac{1}{\phi} \frac{d\omega}{d\phi} - \frac{\omega}{\phi^2} \right) (\nabla\phi)^2, \quad (4)$$

$$\nabla_\nu T_\mu^\nu = 0, \quad (5)$$

where ∇_μ denotes the covariant derivative defined by the $g_{\mu\nu}$, $\square \equiv g^{\mu\nu} \nabla_\mu \nabla_\nu$, and T_μ^ν is the matter stress energy tensor defined as follows

$$T^{\mu\nu} \equiv \frac{2}{\sqrt{-g}} \frac{\delta S_m[\psi, g_{\mu\nu}]}{\delta g_{\mu\nu}}. \quad (6)$$

The energy-momentum conservation is satisfied as Eq.(5) because ordinary matter fields do not directly couple to the scalar field. Combining Eqs.(3)and(4), the equation of motion for ϕ becomes

$$\square\phi = \frac{1}{2\omega + 3} \left\{ 8\pi G T_\mu^\mu - \frac{d\omega}{d\phi} (\nabla\phi)^2 \right\}. \quad (7)$$

B. Background cosmological equation

The unperturbed cosmological spacetime metric is

$$ds^2 = a^2(\eta) (-d\eta^2 + \gamma_{ij} dx^i dx^j), \quad (8)$$

where γ_{ij} is the metric on the comoving homogeneous isotropic 3-space of a constant spatial curvature K . The components of the unperturbed stress energy tensor are

$$T_0^0 = -\rho, \quad T_i^0 = 0, \quad T_j^i = p\gamma_j^i, \quad (9)$$

where ρ and p are the total energy density and pressure, respectively. The background evolution equations are

$$\rho' = -3\frac{a'}{a}(\rho + p), \quad (10)$$

$$\left(\frac{a'}{a}\right)^2 + K = \frac{8\pi G\rho a^2}{3\phi} - \frac{a'\phi'}{a\phi} + \frac{\omega}{6}\left(\frac{\phi'}{\phi}\right)^2, \quad (11)$$

$$\phi'' + 2\frac{a'}{a}\phi' = \frac{1}{2\omega + 3}\left\{8\pi G a^2(\rho - 3p) - \phi'^2 \frac{d\omega}{d\phi}\right\}, \quad (12)$$

where the prime denotes a derivative with respect to η . Although Eq.(10) is the same as that in Einstein gravity as noted previously, the expansion rate a'/a is given by Eq.(11). Non-relativistic matter always contributes to the first term in the right hand side of Eq.(12). The requirement that today's gravitational constant be in agreement with Newton's constant determines the present value of ϕ as

$$\phi_0 = \frac{4 + 2\omega_0}{3 + 2\omega_0}, \quad (13)$$

where ϕ_0 and ω_0 denote the present value of ϕ and $\omega(\phi)$, respectively.

III. SCALAR-TENSOR COSMOLOGICAL PERTURBATION

Following the gauge invariant formulation of the cosmological perturbation theory in Einstein gravity [21],[22], we formulate the gauge invariant perturbation theory in the scalar-tensor gravity.

A. Perturbed quantities

Perturbations of scalar quantities can be expanded by the harmonic functions Y defined as

$$(\Delta + k^2)Y = 0, \quad (14)$$

where $-k^2$ represent their eigen values of Laplace-Beltrami operator Δ on the comoving homogeneous 3-space. Scalar type components in perturbations of vector quantities are expanded by

$$Y_i \equiv -k^{-1}Y_{|i}, \quad (15)$$

where $|_i$ denotes a covariant derivative associated with γ_{ij} . Those in perturbations of tensor quantities are expanded by

$$Y\gamma_{ij} \quad (16)$$

and

$$Y_{ij} \equiv (k^{-2}Y_{|ij} + \frac{1}{3}\gamma_{ij}Y), \quad (17)$$

which correspond to the trace and the traceless part, respectively. In this paper, we will omit the summation symbols and the eigenvalue indices because there is no coupling among the different k -modes. Denoting the perturbed metric by $\tilde{g}_{\mu\nu}$, the components of the perturbed metric are written as

$$\tilde{g}_{00} = -a^2(1 + 2AY), \quad (18)$$

$$\tilde{g}_{0j} = -a^2BY_j, \quad (19)$$

$$\tilde{g}_{ij} = a^2\{(1 + 2H_L Y)\gamma_{ij} + 2H_T Y_{ij}\}. \quad (20)$$

The perturbed scalar field is

$$\tilde{\phi} = \phi + \chi Y. \quad (21)$$

The perturbed energy momentum tensor \tilde{T}_ν^μ has the following components:

$$\tilde{T}_0^0 = -\rho(1 + \delta Y), \quad (22)$$

$$\tilde{T}_j^0 = (\rho + p)(v - B)Y_j, \quad (23)$$

$$\tilde{T}_j^j = -(\rho + p)vY^j, \quad (24)$$

$$\tilde{T}_j^i = p\{(1 + \pi_L Y)\gamma_j^i + \pi_T Y_j^i\}, \quad (25)$$

where δ , v , π_L and π_T are the perturbations of the energy density, the spatial velocity and the isotropic and the anisotropic pressure, respectively. All of the above perturbation quantities are functions only of time. When we consider the background and the perturbed universe, there is gauge freedom to fix the correspondence between the spacetime points in the two spacetimes. Denoting a scalar type infinitesimal gauge transformation by the vector

$$\xi^\mu = (TY, LY^j), \quad (26)$$

where T and L are arbitrary functions of time which has the same order as perturbation variables, we obtain the changes of perturbations under the gauge transformation as

$$\bar{A} = A - T' - (a'/a)T, \quad (27)$$

$$\bar{B} = B + L' + kT, \quad (28)$$

$$\bar{H}_L = H_L - (k/3)L - (a'/a)T, \quad (29)$$

$$\bar{H}_T = H_T + kL, \quad (30)$$

$$\bar{\delta} = \delta - (\rho'/\rho)T, \quad (31)$$

$$\bar{v} = v + L', \quad (32)$$

$$\bar{\pi}_L = \pi_L - (p'/p)T, \quad (33)$$

$$\bar{\pi}_T = \pi_T, \quad (34)$$

and

$$\bar{\phi} = \phi - \phi'T, \quad (35)$$

where the variables with bar represent the gauge transformed values. To treat the evolution of perturbations without unphysical gauge modes, we deal only

with gauge-invariant variables. We can construct gauge-invariant variables by combining perturbation variables. For one perturbation variable, there are several gauge invariants each of which corresponds to the perturbation in a specific gauge. Here, we introduce two gauge invariants for each of the metric, the scalar field and the density perturbations. The one denoted by subscript s corresponds to the perturbation in the Newtonian shear free gauge (where $H_T = B = 0$). The other denoted by subscript c corresponds to the perturbation in the total matter comoving gauge (where $B = v$). Let us proceed to the definition. We can employ two independent variables Ψ and Φ for metric perturbations. The gauge invariant perturbation variables associated with the (0-0) component of the metric are defined as

$$\Psi_s \equiv A + k^{-1}(a'/a)(B - k^{-1}H_T') + k^{-1}(B' - k^{-1}H_T''), \quad (36)$$

$$\Psi_c \equiv A + k^{-1}(a'/a)(B - v) + k^{-1}(B' - v'). \quad (37)$$

These correspond to the perturbations of the gravitational potential in the two gauges. On the other hand, the gauge invariants associated with the spatial component of the metric are

$$\Phi_s \equiv H_L + \frac{1}{3}H_T + k^{-1}(a'/a)(B - k^{-1}H_T'), \quad (38)$$

$$\Phi_c \equiv H_L + \frac{1}{3}H_T + k^{-1}(a'/a)(B - v), \quad (39)$$

which represent the perturbations of the intrinsic spatial curvature in the two gauges. Similarly we introduce two gauge invariants of the scalar field perturbation

$$X_s \equiv \chi - k^{-1}\phi'(k^{-1}H_T' - B), \quad (40)$$

$$X_c \equiv \chi - k^{-1}\phi'(v - B). \quad (41)$$

The gauge invariants of the energy momentum tensor perturbations are defined as follows:

$$\Delta_s \equiv \delta + 3(1+w)(a'/a)k^{-1}(k^{-1}H_T' - B), \quad (42)$$

$$\Delta_c \equiv \delta + 3(1+w)(a'/a)k^{-1}(v - B), \quad (43)$$

$$V \equiv v - k^{-1}H_T', \quad (44)$$

$$\Gamma \equiv \pi_L - \frac{c_s^2}{w}\delta, \quad (45)$$

$$\Pi \equiv \pi_T, \quad (46)$$

where

$$w \equiv p/\rho, \quad (47)$$

$$c_s^2 \equiv p'/\rho'. \quad (48)$$

The conventional photon temperature fluctuation variable is

$$\Theta_0 = \frac{1}{4}\Delta_{s\gamma}, \quad (49)$$

where the subscript γ means the photon component.

B. Perturbation equation

The perturbation equations of Eq.(3) are

$$\begin{aligned} & \frac{2}{a^2} \left[3 \left(\frac{a'}{a} \right)^2 \Psi_s - 3 \frac{a'}{a} \Phi_s' - (k^2 - 3K) \Phi_s \right] \\ &= -\frac{8\pi G}{\phi} \rho \Delta_s + \frac{3}{a^2 \phi} X_s \left\{ \left(\frac{a'}{a} \right)^2 + K \right\} - \frac{1}{a^2 \phi} \left[\left\{ 6 \left(\frac{a'}{a} \right) \Psi_s - 3 \Phi_s' \right\} \phi' - 3 \left(\frac{a'}{a} \right) X_s' - k^2 X_s \right] \\ & \quad - \frac{1}{2a^2} X_s \left(\frac{\phi'}{\phi} \right)^2 \frac{d\omega}{d\phi} + \frac{\omega}{a^2 \phi} \left[\frac{1}{2} \left(\frac{\phi'}{\phi} \right)^2 X_s - \left(\frac{\phi'}{\phi} \right) X_s' + \frac{\phi'^2}{\phi} \Psi_s \right], \end{aligned} \quad (50)$$

$$\frac{2}{a^2} \left[k \frac{a'}{a} \Psi_s - k \Phi_s' \right] = \frac{8\pi G}{\phi} (\rho + p) V - \frac{k}{a^2 \phi} \left\{ \left(\frac{a'}{a} \right) X_s + \phi' \Psi_s - X_s' \right\} + \frac{k\omega}{a^2 \phi} \left(\frac{\phi'}{\phi} \right) X_s, \quad (51)$$

$$\begin{aligned}
& \frac{2}{a^2} \left[\frac{a'}{a} \Psi_s' + \left\{ 2 \left(\frac{a'}{a} \right)' + \left(\frac{a'}{a} \right)^2 - \frac{k^2}{3} \right\} \Psi_s - \Phi_s'' - 2 \frac{a'}{a} \Phi_s' - \frac{k^2}{3} \Phi_s + K \Phi_s \right] \\
&= \frac{8\pi G}{\phi} (p\Gamma + \rho c_s^2 \Delta_s) + \frac{1}{a^2 \phi} X_s \left\{ 2 \left(\frac{a'}{a} \right)' + \left(\frac{a'}{a} \right)^2 + K \right\} \\
&\quad - \frac{1}{a^2 \phi} \left[2\phi'' \Psi_s + \phi' \left\{ \Psi_s' + 2 \frac{a'}{a} \Psi_s - 2\Phi_s' \right\} - X_s'' - \frac{a'}{a} X_s' - \frac{2k^2}{3} X_s \right] \\
&\quad + \frac{1}{2a^2} X_s \left(\frac{\phi'}{\phi} \right)^2 \frac{d\omega}{d\phi} - \frac{\omega}{a^2 \phi} \left[\frac{1}{2} \left(\frac{\phi'}{\phi} \right)^2 X_s - \left(\frac{\phi'}{\phi} \right) X_s' + \frac{\phi'^2}{\phi} \Psi_s \right], \tag{52}
\end{aligned}$$

$$- \frac{k^2}{a^2} \left\{ \Phi_s + \Psi_s \right\} = \frac{8\pi G}{\phi} p\Pi + \frac{k^2}{a^2 \phi} X_s. \tag{53}$$

The perturbation equation of Eq.(7) is

$$\begin{aligned}
& X_s'' + 2 \frac{a'}{a} X_s' + k^2 X_s - 2\phi'' \Psi_s - \phi' \left(\Psi_s' + 4 \frac{a'}{a} \Psi_s - 3\Phi_s' \right) \\
&= \frac{a^2}{2\omega + 3} \left[8\pi G \rho \left\{ (1 - 3c_s^2) \Delta_s - 3w\Gamma \right\} - \frac{d^2 \omega}{d\phi^2} X_s a^{-2} \phi'^2 - 2 \frac{d\omega}{d\phi} a^{-2} (\phi' X_s' - \phi'^2 \Psi_s) - 2 \frac{d\omega}{d\phi} a^{-2} X_s (\phi'' + 2 \frac{a'}{a} \phi') \right]. \tag{54}
\end{aligned}$$

The perturbation equations of Eq.(5) are

$$\begin{aligned}
\Delta_c' - 3 \left(\frac{a'}{a} \right) w \Delta_c &= -3(1+w) \Phi_c' - (1+w) k V \\
-3 \left(\frac{a'}{a} \right) w \Gamma - 3 \left(\frac{a'}{a} \right) c_s^2 \Delta_c, & \tag{55}
\end{aligned}$$

$$\begin{aligned}
V' + \left(\frac{a'}{a} \right) V &= k \Psi_s \\
+ \frac{k}{1+w} \left\{ c_s^2 \Delta_c + w\Gamma - \frac{2}{3} \left(1 - \frac{3K}{k^2} \right) w\Pi \right\}. & \tag{56}
\end{aligned}$$

These are the same as those in Einstein gravity. Of course, the Boltzmann equations for photons and neutrinos are also not modified. Hence we omit them here.

From Eq.(56), the relation between the potential perturbation and pressure perturbations becomes

$$\Psi_c = - \frac{1}{1+w} \left\{ c_s^2 \Delta_c + w\Gamma - \frac{2}{3} \left(1 - \frac{3K}{k^2} \right) w\Pi \right\}. \tag{57}$$

Employing the total matter gauge variables and using

$$\begin{aligned}
\frac{a'}{a} \Psi_c - \Phi_c' &= K \frac{V}{k} - \frac{1}{2\phi} \left\{ \left(\frac{a'}{a} \right) X_c + \phi' \Psi_c - X_c' \right\} \\
&\quad + \frac{\omega}{2\phi} \left(\frac{\phi'}{\phi} \right) X_c, \tag{58}
\end{aligned}$$

we obtain the alternative expression of Eq.(54) that is

$$\begin{aligned}
& X_c'' + 2 \frac{a'}{a} X_c' + k^2 X_c - 2\phi'' \Psi_c - \phi' \left(\Psi_c' + \frac{a'}{a} \Psi_c \right) + k\phi' \left(1 - \frac{3K}{k^2} \right) V + \frac{3}{2} \frac{\phi'}{\phi} \left\{ \left(\frac{a'}{a} \right) X_c + \phi' \Psi_c - X_c' \right\} - \frac{3\omega}{2} \left(\frac{\phi'}{\phi} \right)^2 X_c \\
&= \frac{a^2}{2\omega + 3} \left[8\pi G \rho \left\{ (1 - 3c_s^2) \Delta_c - 3w\Gamma \right\} - \frac{d^2 \omega}{d\phi^2} X_c a^{-2} \phi'^2 - 2 \frac{d\omega}{d\phi} a^{-2} (\phi' X_c' - \phi'^2 \Psi_c) - 2 \frac{d\omega}{d\phi} a^{-2} X_c (\phi'' + 2 \frac{a'}{a} \phi') \right]. \tag{59}
\end{aligned}$$

Combining Eqs.(50), (51) and (53), we obtain the generalized Poisson equation in the scalar-tensor theory as

follows:

$$\begin{aligned}
-(k^2 - 3K)\Psi_s = & \frac{4\pi G\rho a^2}{\phi} \left(\Delta_c - \frac{2}{\phi} X_c \right) + \frac{1}{4} \left(\frac{\phi'}{\phi} \right)^2 \frac{d\omega}{d\phi} X_c + \frac{2\omega + 3}{4\phi} \left(\frac{\phi'}{\phi} \right) \left\{ X_c' + 3 \left(\frac{a'}{a} \right) X_c - \phi' \Psi_c \right\} \\
& + (k^2 - 3K) \left\{ \frac{8\pi G}{\phi} \left(\frac{a}{k} \right)^2 p\Pi + \frac{X_c}{2\phi} + \frac{1}{2k} \frac{\phi'}{\phi} V \right\}. \quad (60)
\end{aligned}$$

The gravitational redshift factor in the scalar-tensor theory is written as:

$$\Phi_s - \Psi_s = \Upsilon_\psi + \Upsilon_\phi, \quad (61)$$

where

$$\Upsilon_\psi \equiv \frac{8\pi G}{\phi} \left(\frac{a}{k} \right)^2 \left\{ \left(1 - \frac{3K}{k^2} \right)^{-1} \rho \Delta_c + p\Pi \right\}, \quad (62)$$

$$\Upsilon_\phi \equiv (k^2 - 3K)^{-1} \left[-\frac{16\pi G\rho a^2}{\phi} \frac{X_c}{\phi} + \frac{1}{2} \left(\frac{\phi'}{\phi} \right)^2 \frac{d\omega}{d\phi} X_c + \frac{2\omega + 3}{2\phi} \left(\frac{\phi'}{\phi} \right) \left\{ X_c' + 3 \left(\frac{a'}{a} \right) X_c - \phi' \Psi_c \right\} \right]. \quad (63)$$

Υ_ψ and Υ_ϕ are the contribution of matter perturbations and the scalar field perturbation, respectively. If the background spacetime and the initial conditions for perturbations are given, we can solve the above equations. The initial conditions for perturbations (solutions on a superhorizon scale in the radiation-dominated epoch) are discussed in the next section.

IV. NUMERICAL CALCULATION

Let us now numerically solve the evolution of the background universe and perturbations. We apply our formulation to flat Λ CDM models. The matter components are baryons, cold dark matters, photons, and three species of massless neutrinos. (In cold dark matter dominated models, massive neutrinos do not significantly change the evolution of ϕ .) In our numerical calculations, the functional form of $\omega(\phi)$ is

$$2\omega + 3 = \left\{ \alpha_0^2 - \beta \ln(\phi/\phi_0) \right\}^{-1}. \quad (64)$$

This $\omega(\phi)$ corresponds to the harmonic effective potential of the scalar field in the Einstein conformal frame. α_0 and β in Eq.(64) are today's potential gradient and curvature, respectively [14],[15]. If $\beta = 0$, this model is reduced to the Brans-Dicke theory. Moreover, the model with $\alpha_0 \rightarrow 0, \beta = 0$ is Einstein gravity. To realize the cosmological attractor mechanism, we treat the parameter region $\beta \geq 0$ in this paper. Although some parameter region is already excluded by solar-system experiments and the BBN analysis, we often adopt unrealistically large values of α_0 and β to see the qualitative parameter dependence of the results.

A. Boundary condition

First, we describe the boundary conditions for background variables. We employ the conventional definitions of cosmological parameters

$$\Omega_0 \equiv \rho_0/\rho_c, \quad \Omega_K \equiv -K/a_0^2 H_0^2, \quad \rho_c \equiv 3H_0^2/8\pi G. \quad (65)$$

Unless otherwise noted, we fix today's baryon density ($\Omega_b \equiv \rho_{b0}/\rho_c$) and Hubble parameter (h) to 0.03 and 0.7, respectively. (In this paper, we do not discuss the light element abundance synthesized via BBN in the scalar-tensor cosmology. The helium mass fraction is fixed at 23% in our calculations.) Then, the density of CDM is determined by $\Omega_{c0} = \Omega_0 - \Omega_{b0}$. In the scalar-tensor theory, the relation between the cosmological parameters is as follows

$$\frac{\Omega_0}{\phi_0} + \Omega_K - S + \frac{\omega(\phi_0)}{6} S^2 = 1, \quad (66)$$

where $S \equiv \dot{\phi}_0/\phi_0 H_0$ and $\dot{\phi} = \frac{1}{a} \frac{d\phi}{d\eta}$. We set Ω_K in the above equation to be zero since we treat only flat models. As mentioned in Section II, ϕ_0 must satisfy Eq.(13). In the scalar-tensor theory, Ω_0 is not necessarily unity even in flat Λ CDM models. There exists the degree of freedom to determine the amplitude of the vacuum solution mode of ϕ' ($\propto a^{-2}(2\omega + 3)^{-\frac{1}{2}}$) at the present time. As in the precedent study [20], we assume that such a mode is negligible ever since the initial time of our calculations. Then, from the particular solution during the matter dominated epoch [14], the relation that Ω_0 and S must satisfy in $0 \leq \beta < 3/8$ models becomes

$$\Omega_0 = \frac{(1 + \alpha_0^2)(1 - \partial\varphi_0^2/3)}{(1 + \alpha_0\partial\varphi_0)^2}, \quad S = -\frac{2\alpha_0\partial\varphi_0}{(1 + \alpha_0\partial\varphi_0)}, \quad (67)$$

where $\partial\varphi_0 = -3\alpha_0(1-r)/(4\beta)$ and $r = (1 - 8\beta/3)^{1/2}$. In this paper, we set the initial time $z \sim 10^8$ so that the modes observed today as large scale structures are still before their horizon entry. Moreover, the energy of electrons and positrons already have no effect on ϕ evolution at that time. We search for the numerical solution of ϕ satisfying the above boundary conditions by iterating the initial value of ϕ, ϕ_{ini} . The initial value of ϕ' to a given ϕ_{ini} which is composed of the particular solution is

$$\phi'_{ini} = \frac{3\phi_{ini}}{4\omega_{ini} + 6} \frac{a}{a_{eq}} \left(\frac{8\pi G \rho a^2}{3\phi_{ini}} \right)^{\frac{1}{2}}. \quad (68)$$

Here we assume that ϕ (and $\omega(\phi)$) are almost constant and the ϕ' terms in Eq.(11) are negligible at the initial time. In fact, the factor a/a_{eq} extremely damps its amplitude and this is consistent with these assumptions.

Next, the initial conditions for perturbation variables should be noted. Here, the initial condition means the solution on a superhorizon scale in the radiation-dominated epoch. To obtain the initial solution of X_c , we employ the similar procedure as applied to ϕ' . In addition, for matter perturbations, we adopt the same adiabatic initial conditions as those in Einstein gravity. Then, the homogeneous solution of Eq.(59) consists of a constant and a decaying mode, whose contribution to the gravitational potential perturbation decreases with time. Neglecting them and using the initial solutions for matter perturbations, we obtain the growing particular solution of X_c that is

$$X_c = \frac{3\phi_{ini}}{32\omega_{ini} + 48} \frac{a}{a_{eq}} \frac{5 + 3f_\nu}{7 + 5f_\nu} \Delta_c, \quad (69)$$

where $f_\nu = \rho_\nu/\rho_\gamma$. This solution contains neutrino anisotropic stress contribution. Consistently, this initial solution of X_c does not modify the initial solutions for matter perturbations because the contribution of X_c (and ϕ') to metric perturbations is at most comparable to that of CDM perturbation $O(a/a_{eq})$.

B. Background

Here we compare the time evolution of background variables in some typical models.

Fig.1 shows the α_0 dependence of ϕ evolution and Fig.2 shows the β dependence of it. ϕ is frozen during the radiation-dominated epoch and begins to roll down at the matter-radiation equality time to realize the Newtonian gravitational constant at the present. As increasing α_0 or β , we obtain smaller initial ϕ . In the Brans-Dicke (constant ω) models, the late time slope is monotonic. On the other hand, in the attractor (variable ω) models, the time variation of $\omega(\phi)$ which regulates the amplitude of ϕ' (proportional to $(2\omega + 3)^{-1}$) causes a steep slope immediately after the equality time and a gentle slope near the present. For reference, the $\Omega_0 h^2$ dependence of ϕ evolution is illustrated in Fig.3. The shift of equality time

simply decreases the initial value of ϕ without altering the late time evolution. Now, even if we employ a vacuum dominated model, the period from vacuum domination is quite short in units of $\ln a$ and hence the only influence on ϕ is to decrease in today's matter density. Thus, in a vacuum dominated model, the history of ϕ is modified only before the equality time as the low density SCDM models in Fig.3.

Fig.4 compares the time evolution of $\omega(\phi)$ in the attractor models. ω can vary only after the equality time because, even in variable ω models, the variation of ϕ is suppressed before the equality time. The late time power-law behavior is well described by

$$2\omega + 3 \simeq (2\omega_0 + 3) \left(\frac{a}{a_0} \right)^{\frac{3}{2}(1-r)}. \quad (70)$$

r is defined in the previous section.

Fig.5 illustrates the time evolution of $\phi'/(a'/a)$ in the attractor models which also represents the variation of ϕ during a logarithmic interval of $1+z$. (It should be noted about α_0 dependence that the whole amplitude of these curves is nearly proportional to α_0^2 .) The variability of ϕ is summarized as follows:

$$\phi' \left(\frac{a'}{a} \right)^{-1} = \frac{d\phi}{d \ln a} \sim \begin{cases} \frac{1}{\omega} \frac{a}{a_{eq}} & \text{RD} \\ \frac{1}{\omega} & \text{MD} \end{cases} \quad (71)$$

The initial slope represents the ratio of matter energy density to radiation energy density. Then, the motion of ϕ is negligible and does not affect the spacetime metric through either of the minimal and the non-minimal coupling. Hence, the scalar-tensor gravity effectively behaves like Einstein gravity and the only difference is the magnitude of the gravitational coupling "constant". The larger gravitational constant results in the larger expansion rate and therefore the smaller horizon length. On the other hand, in the matter-dominated epoch, ϕ can move in the absence of the suppression factor $O(a/a_{eq})$. As a result, the time variation of ϕ changes the nature of gravity qualitatively. For example, a is not proportional to η^2 . Especially in the attractor models, such effects appear only in the intermediate epochs between the equality and the present because the deviation from Einstein gravity is in proportion to $\omega(\phi)^{-1}$. Thus, the effect of scalar field dynamics is most significant around the equality time.

C. Perturbation

In this section, the evolution of perturbation variables is shown. When comparing the perturbation spectra, we adopt scale invariant models without discussing the generation mechanism of perturbations. The amplitude of the curvature perturbation (Φ_s) in each model is initially indistinguishable. Hence, a comparison between models shows directly the difference in their evolution.

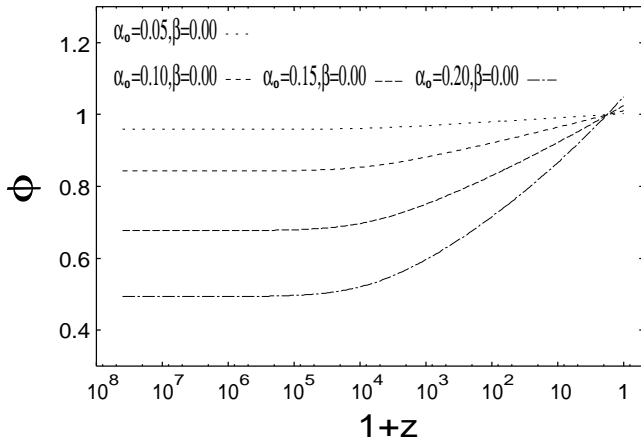


FIG. 1: The time evolution of ϕ in the Brans-Dicke models with SCDM parameters where Ω_0 is determined by Eq.(67). The discrepancy at the present is due to the different ω .

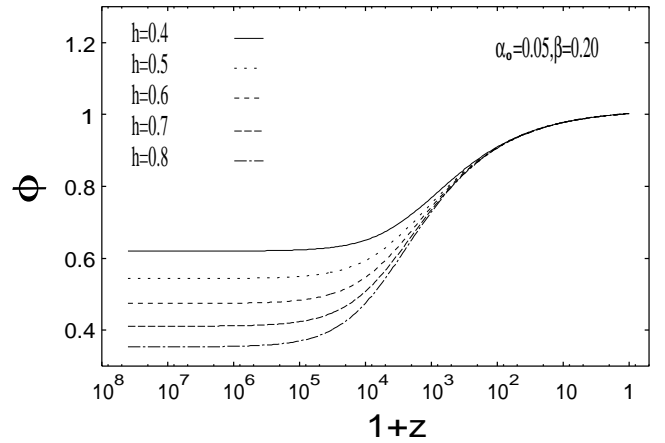


FIG. 3: The density dependence of ϕ history in the attractor models with SCDM parameters. Ω_0 is determined by Eq.(67) and $\Omega_b h^2$ is fixed to 0.0147.

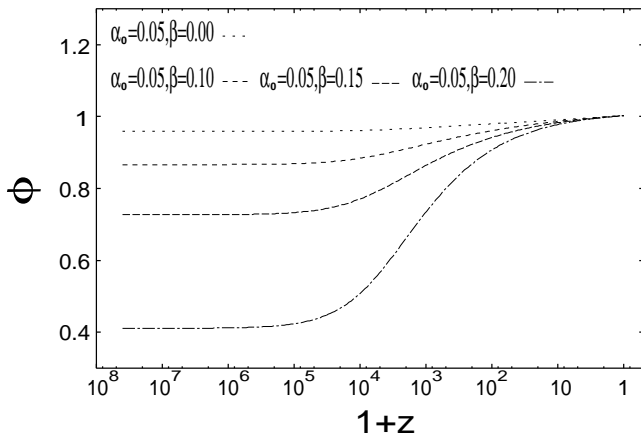


FIG. 2: The time evolution of ϕ in the attractor models with SCDM parameters where Ω_0 is determined by Eq.(67). Note that the variation of ω makes an inflection point around the equality time (cf. Fig.5). The alignment at the present time is due to the equality of $\omega(\phi_0)$.

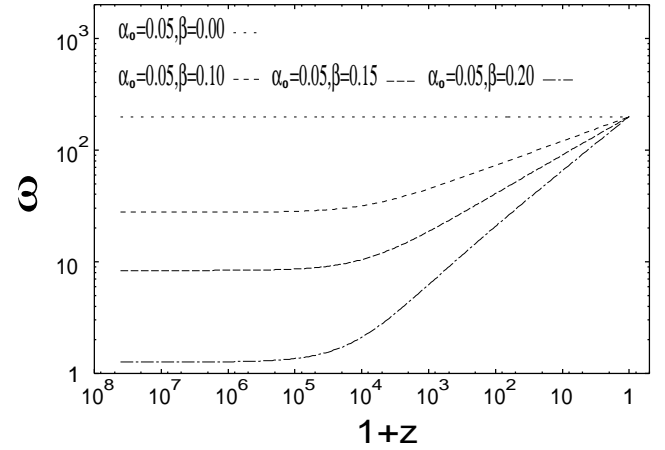


FIG. 4: The time evolution of $\omega(\phi)$ in the attractor models with SCDM parameters.

1. Scalar field perturbation

Fig.6 and Fig.7 show the early and the late time behavior of the scalar field perturbation, respectively. The analytic estimation is presented in Appendix. Before the horizon entry, the scalar field fluctuation cumulates around the dense region and X_c always grows. Then, the amplitude is approximately proportional to the factor $\omega(\phi)^{-1}$ which regulates the nonminimal interaction. While, after the horizon entry, the field fluctuation flows out and its growth is suppressed. Then, X_c oscillates at the same frequency as radiation fluid in the radiation-dominated epoch or converges to some amplitude in the matter-dominated epoch.

As in the background, the contribution of the scalar

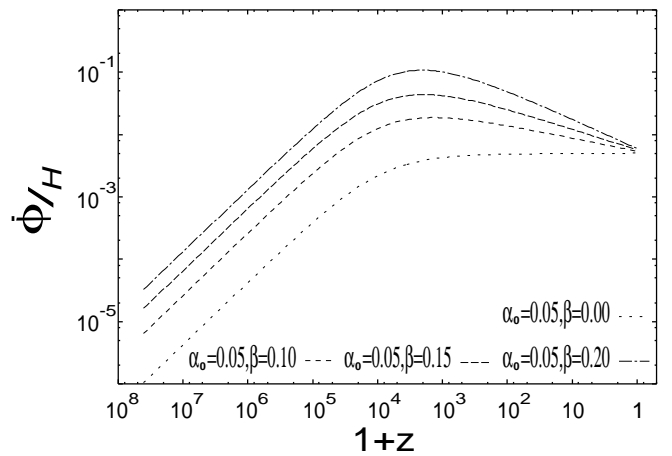


FIG. 5: The time evolution of $\dot{\phi}/H$ in the attractor models with SCDM parameters, where $\dot{\phi} = \frac{1}{a} \frac{d}{d\eta} \phi$. The maximums correspond to the inflection points in Fig.2.

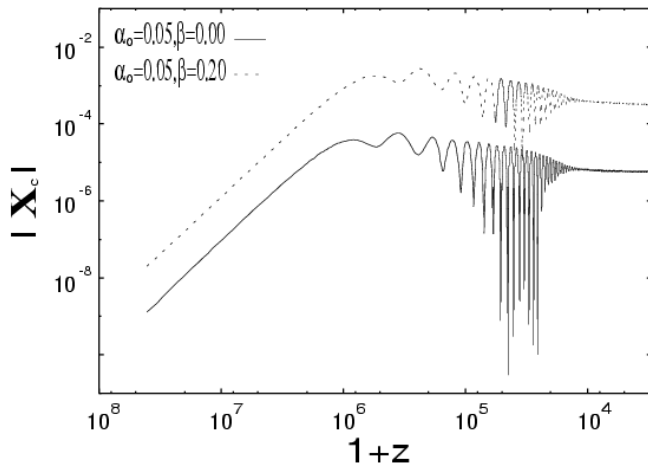


FIG. 6: The early evolution of X_c on a scale $k = 10 \text{ Mpc}^{-1}$ in the scalar-tensor models with SCDM parameters. Normalization is arbitrary. Their amplitude is proportional to ω^{-1} (or ω_{ini}^{-1}). The discrepancy of their horizon entry times is due to the difference in $\phi_{initial}$.

field to the metric is initially negligible. Until the mode enters the horizon, it becomes larger and reaches $O(\omega_{ini}^{-1})$ fraction around the equality time. It is shown in Fig.8 and Fig.9 where the feature of the largest scale mode is quite similar to the respective curve in Fig.5. Immediately after the horizon entry, the contribution suddenly drops and becomes negligible. This potential drop at the horizon entry is the characteristic event caused by the scalar field fluctuation especially in the matter-dominated epoch during which the horizon entry does not involve the potential decay in the Einstein model. Because of the late time convergence to Einstein gravity, large scale modes, as well as small scale modes which enter the horizon long before the equality time, are not affected by the scalar fluctuation in the attractor model.

2. Metric perturbation

The metric evolution directly affects the evolution of matter perturbations. Its evolution can be seen through the observations of the present matter structures. For example, the turnover scale in the matter power spectrum corresponds to the horizon scale at the equality time. CMB observations provide more detailed information about the gravity evolution. Therefore, we pick up some scale modes which appear on the CMB anisotropy spectrum as the characteristic structure, namely the modes corresponding to the acoustic peaks. The evolution of the first and the second acoustic peak modes at the decoupling time is displayed in Fig.10 and Fig.11 where the large scale limit modes are also compared for reference. The initial behavior is model independent because the scalar-tensor gravity behaves like Einstein gravity. In the Brans-Dicke model, the late time evolution, except for

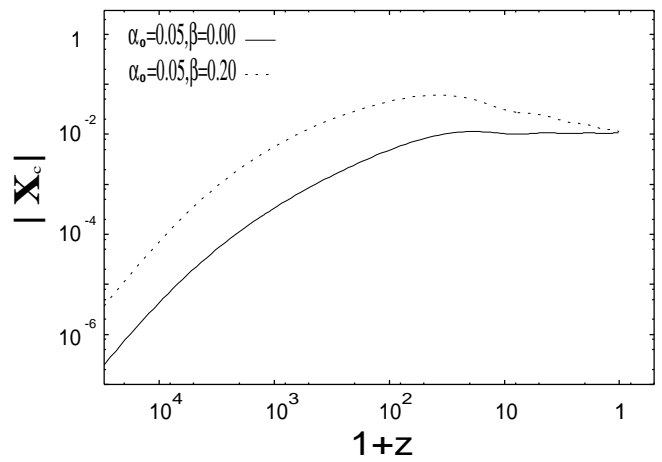


FIG. 7: The late time evolution of X_c on a scale $k = 0.003 \text{ Mpc}^{-1}$ in the scalar-tensor models with SCDM parameters. Normalization is arbitrary. These modes enter the horizon around $z \simeq 10^2$. Their amplitude is proportional to $\omega(\phi)^{-1}$ and the convergence at the present represents the same ω_0^{-1} .

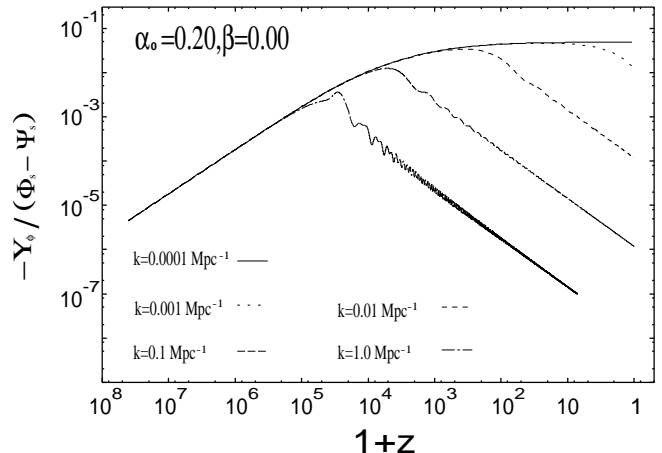


FIG. 8: The evolution of $-\Upsilon_\phi / (\Phi_s - \Psi_s)$ on some typical scales in the Brans-Dicke model with SCDM parameters. Small scale modes are not affected by the scalar fluctuation.

the horizon entry, is flat as discussed in Appendix. Also in the attractor model, the late time evolution gradually becomes flat because of the convergence to Einstein gravity. The large scale limit mode especially is not affected by the difference in the horizon entry and its late time deviation is determined by $\omega(\phi)^{-1}$. After the equality, the decay widths of peak modes at a time generally become smaller in the scalar-tensor models than those in the Einstein model (see e.g. the second peak mode in Fig.10 or Fig.11). We point out two reasons for it. One reason is that the non-relativistic matter amount (Ω_0) is larger in the scalar-tensor models. The relative contribution of radiation to metric perturbations is smaller at the same z and hence the decay caused by radiation

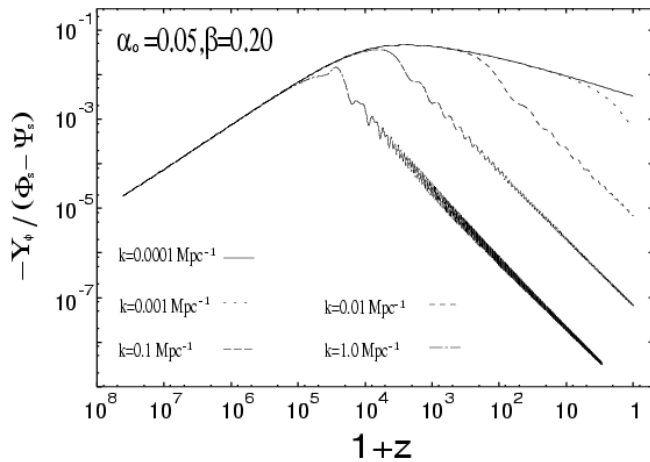


FIG. 9: The evolution of $-\Upsilon_\phi/(\Phi_s - \Psi_s)$ on some typical scales in the attractor model with SCDM parameters. There exists the scale which is most affected by the scalar fluctuation.

pressure becomes smaller. The other reason is the motion of ϕ . As explained in Fig.12, if ϕ is constant, a peak mode in each model enters the horizon at the same time. However, since ϕ moves with time after the equality, the entry time of the peak mode in the scalar-tensor model is shifted to lower z . This time lag also makes the decay width smaller. Furthermore, during the early phase of potential decay (approximately from the horizon entry up to the first maximum compression of photon fluid), the contribution of the scalar induced decay occurring coherently to the decay deriving from radiation pressure is not negligible. For instance, the potential of the first peak mode in Fig.10 or Fig.11 catches up with that in the Einstein model around $z \sim 10^3$.

The late time evolution of the power spectra of the gravitational potential in the large scale in the scalar-tensor models is displayed in Fig.13 and Fig.14. Since that scale enters the horizon much later after the equality time, the scalar induced potential decay can be clearly seen. As noted above, the decay width is decreasing with time in the attractor model and hence the large scale modes are not affected significantly.

3. Matter perturbation

In the radiation-dominated epoch, the difference in the magnitude of the gravitational constant alone affects matter evolution. It is clearly seen in Fig.15 which exhibits the acoustic oscillation of photon fluid at $z = 10^6$. As explained in Fig.12, the peak mode in each model enters the horizon at the same time due to the constancy of the gravitational constant (ϕ). Therefore, the degree of the peak boost is equal for each model. Parallel transports make these curves identical except in their diffusion cut off. After the gravitational constant begins to vary,

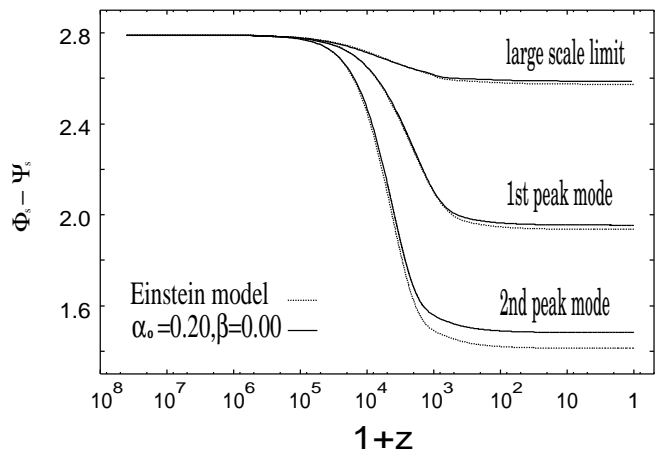


FIG. 10: The evolution of $\Phi_s - \Psi_s$ on some scales in the Einstein and the Brans-Dicke model with SCDM parameters. Normalization is arbitrary.

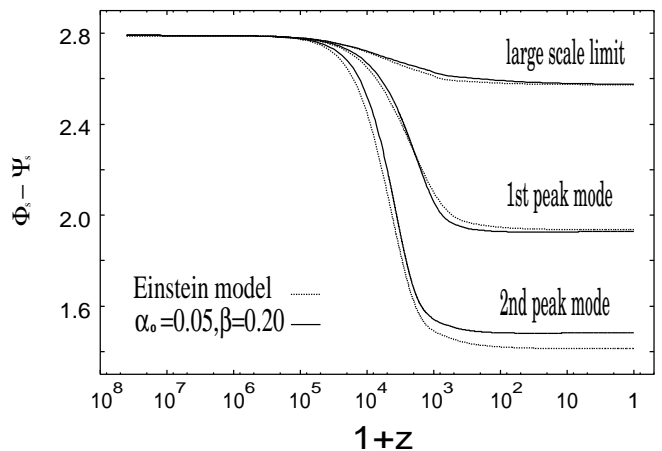


FIG. 11: The evolution of $\Phi_s - \Psi_s$ on some scales in the Einstein and the attractor model with SCDM parameters. Normalization is arbitrary.

the peak heights generally become lower than those in the Einstein model. Exceptionally, during the first acoustic compression, the mode experiences also the enhancement caused by the scalar induced potential decay.

The observable oldest universe is the photon decoupling epoch. Fig.16 and Fig.17 show the photon and the potential power spectra at $z = 1000$. It should be noted that z of the recombination time is not shifted because it is determined almost only by the photon temperature. On very large scales (commonly called Sachs-Wolfe plateau), the fluctuation amplitude in the scalar-tensor models is slightly larger than that in the Einstein model. The deviation represents the value of ω^{-1} at that time. The small scale potential height is, of course, higher in the scalar-tensor models, which implies the smaller horizon length at the equality time. On acoustic peak scales, in addition to peak locations which represent the hori-

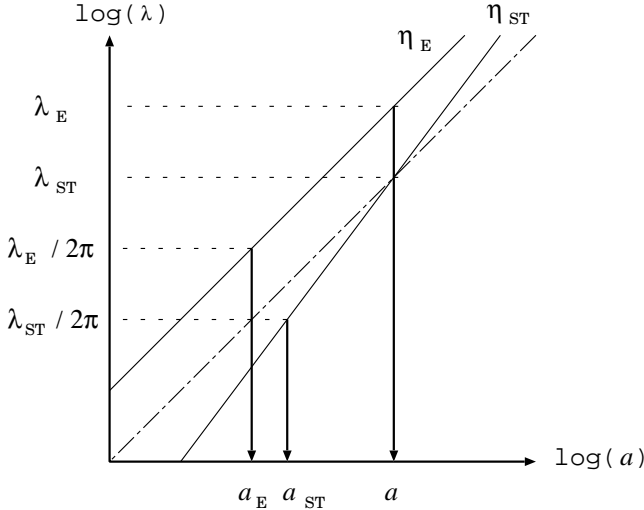


FIG. 12: The schematic diagram illustrating how the variation of ϕ reduces the potential decay width, where $a_0/a = 1+z$. For instance, let λ_E and λ_{ST} be the second peak scales at some redshift in the Einstein and the scalar-tensor model, respectively. Due to the smaller ϕ in the past, the horizon expansion in the scalar-tensor model behaves as lower solid line in the figure rather than dot-dashed line and hence the horizon entry is shifted to lower z than that in the Einstein model.

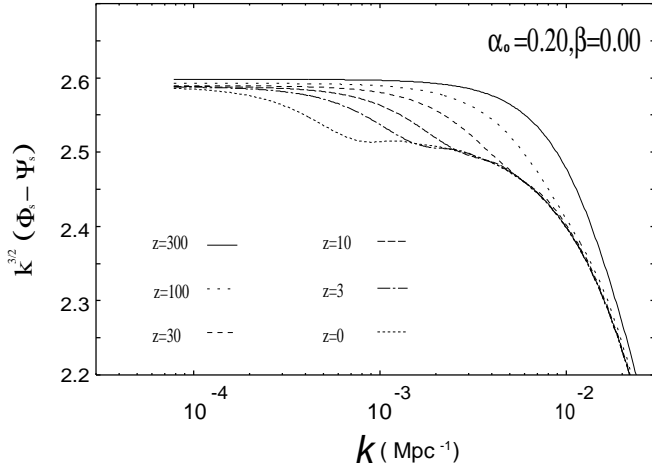


FIG. 13: The power spectra of gravitational potential $\Phi_s - \Psi_s$ at some redshifts in the Brans-Dicke model with SCDM parameters. Normalization is arbitrary. The potential decays to some extent as the mode enters the horizon.

zon length at the time, we can see three features: the first Doppler peak height, the second peak height and the diffusion envelope. Let us begin with the diffusion scale. The diffusion length is also dependent on the horizon length. In fact, it is defined as:

$$l_D = \left(\frac{l_H}{n_e \sigma_T} \right)^{\frac{1}{2}} \Big|_{a=a_{rec}}, \quad (72)$$

where l_H , n_e , and σ_T are horizon length, free electron

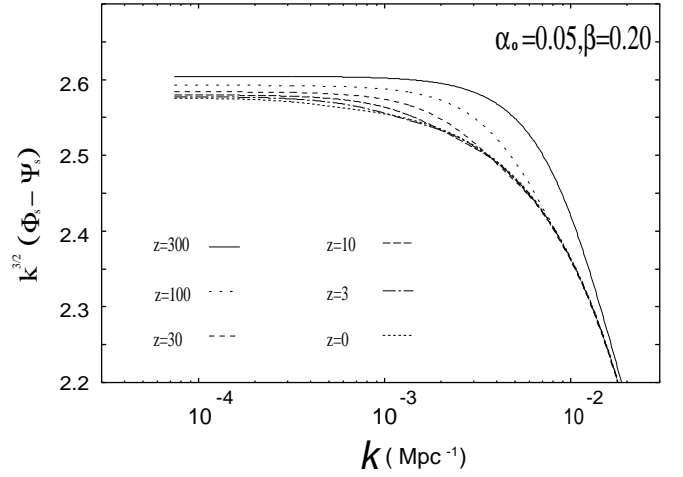


FIG. 14: The power spectra of gravitational potential $\Phi_s - \Psi_s$ at some redshifts in the attractor model with SCDM parameters. Normalization is arbitrary. The decay width becomes smaller as ω becomes larger.

density, and the Thomson scattering cross-section, respectively. And a_{rec} is the scale factor at the beginning of hydrogen recombination. The mean free path is model independent and hence the diffusion efficiency depends only on $l_H^{\frac{1}{2}}$. Therefore, the higher diffusion envelope in the scalar-tensor models also derives from the smaller horizon length. On the other hand, single peak inside the envelope in the scalar-tensor models is lower than that in the Einstein model because the ratio of the peak scales to the diffusion length is, in turn, proportional to $l_H^{-\frac{1}{2}}$. Aside from the diffusion effect, acoustic peak heights in the scalar-tensor models generally become lower after the equality time due to the smaller potential decay of the peak modes. This results in the lower second peak in Fig.16 and Fig.17. This difference in the second peak height indeed originates from the difference in gravity, which can be confirmed by trying different Ω_b models. Concerning the first peak scale, as noted in the previous section, the scalar induced potential decay has non negligible effect. It occurs coherently to ordinary potential decay and makes the total decay width larger. This boosts the first Doppler peak higher because the mode is in its first maximum compression phase at the decoupling time. (Precisely, ordinary potential decay is triggered by a “sound” horizon entry. Thus the degree of this enhancement correlates with the sound velocity of photon-baryon fluid. In larger $\Omega_b h^2$ models, the enhancement of the first peak becomes more significant.)

Also after the decoupling time, the scalar induced potential decay affects matter evolution at the horizon entry. It is found that it makes a bump in the potential transfer function (Fig.13 and Fig.14) and the photon root mean square fluctuation ($|\Theta_0 + \Psi_s|_{rms}^2 = |\Theta_0 + \Psi_s|^2 + \sum \frac{\Theta_l^2}{2l+1}$) spectrum (Fig.18) around the horizon scale of the time. In Fig.18, the amplitude on super

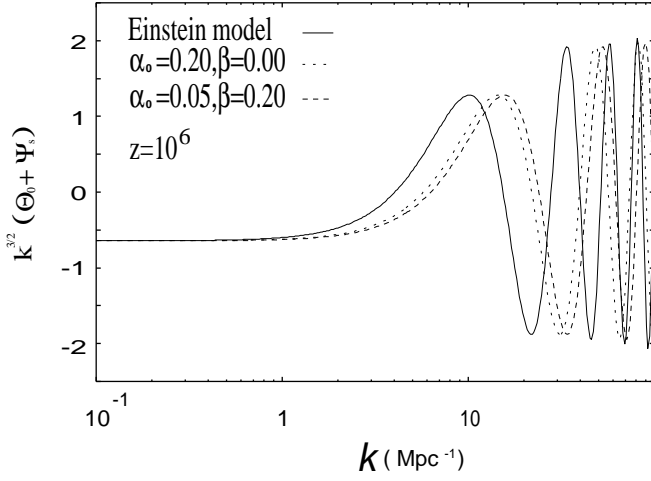


FIG. 15: The power spectra of effective temperature fluctuation at $z = 10^6$ in the Einstein and the scalar-tensor models with SCDM parameters. Normalization is arbitrary. Before ϕ begins to move, the only difference is that the gravitational "constant" in the scalar-tensor models is larger than Newton's constant.

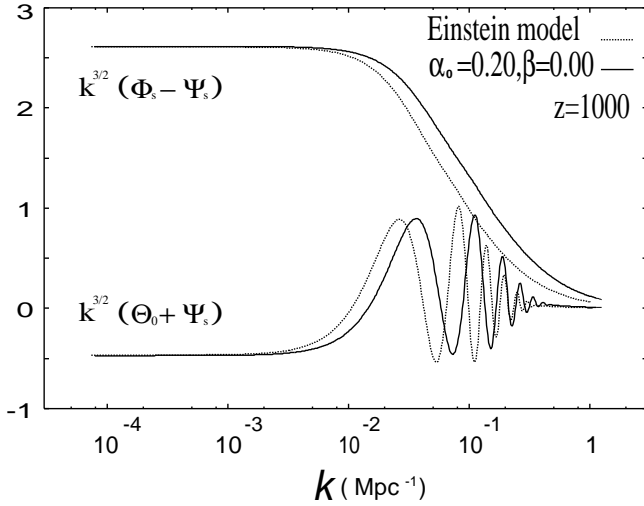


FIG. 16: The power spectra of effective temperature fluctuation $\Theta_0 + \Psi_s$ and gravitational potential $\Phi_s - \Psi_s$ at $z = 1000$ in the Einstein and the Brans-Dicke model with SCDM parameters. Normalization is arbitrary.

present horizon scales is higher than that in the Einstein model by ω_0^{-1} . However, the amplitude deviation inside the horizon ($k \sim 10^{-3} \text{ Mpc}^{-1}$) is somewhat reduced by this ISW (integrated Sachs-Wolfe) effect. On the other hand, the temperature fluctuation at the foot of the first Doppler peak which is blue shifted at the decoupling time is enhanced by the effect. This uplift is not so clear on the figure due to the smaller sound horizon length at the decoupling. In the attractor model, this effect is not so large on Sachs-Wolfe scales as on the scales around the first Doppler peak because the decay width is proportional to $\omega(\phi)^{-1}$ at the horizon entry.

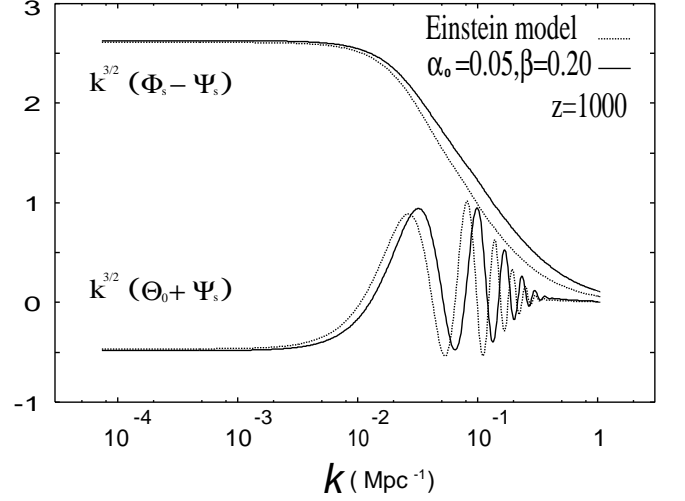


FIG. 17: The power spectra of effective temperature fluctuation $\Theta_0 + \Psi_s$ and gravitational potential $\Phi_s - \Psi_s$ at $z = 1000$ in the Einstein and the attractor model with SCDM parameters. Normalization is arbitrary.

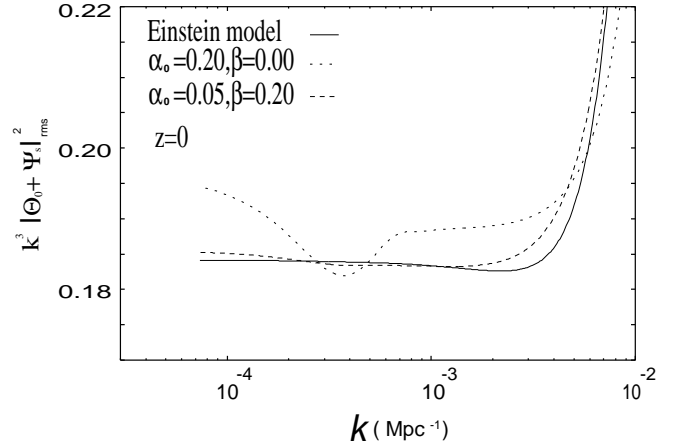


FIG. 18: The large scale power spectra of photon rms temperature fluctuation at the present in the Einstein and scalar-tensor models with SCDM parameters. Normalization is arbitrary. The scalar induced potential decay makes an uplift at the foot of the first Doppler peak and a bump around the present horizon scale.

V. OBSERVATIONAL QUANTITIES

Observations of the large scale structure of the Universe and the CMB anisotropies are the strong tools to constrain the theories of primordial fluctuation evolution. Adopting scale invariant initial spectra, we present the matter power spectra and the CMB temperature anisotropy spectra based on the numerical calculations in the previous section.

Before proceeding to the resulting spectra, we comment on the normalization. We find that, if the initial curvature perturbations are normalized to the same am-

plitude, the temperature anisotropy power on COBE normalization angular scales is almost model independent. However, this does not necessarily imply that the large scale power on the matter power spectrum is also model independent. The conservation of the adiabatic relation ($\Delta_{cr}/\Delta_{cm} = 4/3$) during when the mode is before the horizon entry is model independent. Here, the subscript r and m means a radiation and a non-relativistic component, respectively. According to Appendix, this fact indicates that, in the Brans-Dicke model, the familiar Sachs-Wolfe relation is modified as follows:

$$\Theta_0 + \Psi_s = \frac{1}{3} \left(1 + \frac{2}{3\omega} \right) \Psi_s + O(\omega^{-2}). \quad (73)$$

This is just an example. The actual modification also includes the contribution of the ISW effect and others.

A. Matter power spectrum

On subhorizon scales in the radiation-dominated epoch, the growth of density perturbations is inhibited by radiation pressure. After the transition from radiation domination to matter domination, perturbations on all length scales can grow by gravity. Hence in the matter perturbation spectrum, there exists the imprint of the horizon scale at the matter-radiation equality time. We can see the difference in the horizon scales at the equality time in Fig.1 and Fig.2. The matter power spectra in the Einstein model and the scalar-tensor models are shown in Fig.19 and Fig.20. It has been pointed out (in the context of Brans-Dicke cosmology [19]) that the variation of ϕ results in the larger expansion rate and then the turnover scale of the present-day matter power spectrum shifts to the smaller scale, accordingly there is more small scale power. It is found from the figures that large scale power deviates from its Einstein counterpart in proportion to ω_0^{-1} .

B. CMB temperature anisotropy spectrum

The COBE normalized CMB anisotropy spectra are compared in Fig.21 and Fig.23. Fig.22 and Fig.24 show their component decomposition which is calculated by directly projecting the inhomogeneity spectra at the decoupling time into l space.

First, we mention the shift of characteristic angular scales. The acoustic peak location (sound horizon scale) and the diffusion cut off scale are dependent on the horizon length at the decoupling time. Since the matching condition of ϕ_0 constricts the deviation of the present horizon length, these angular scales directly represent the horizon length at the decoupling. Therefore, the shift of peak locations to smaller angular scales is due to the large gravitational constant at the decoupling. Although the damping scale also depends on the horizon length, it is

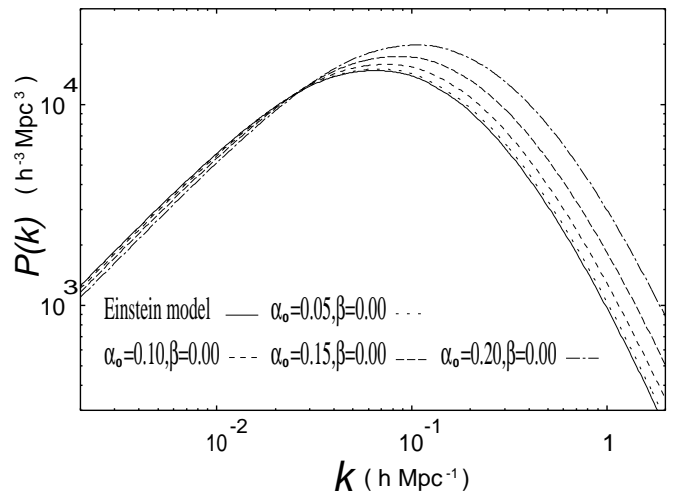


FIG. 19: The COBE normalized matter power spectra in the Brans-Dicke models with SCDM parameters. The turnover scale shifts according to the horizon scale at the matter radiation equality time. The difference in ω also affects the large scale amplitude.

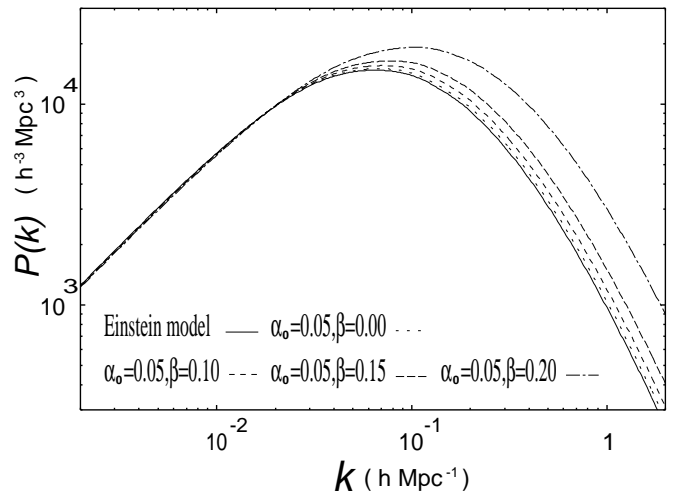


FIG. 20: The COBE normalized matter power spectra in the attractor models with SCDM parameters. The turnover scale shifts according to the horizon scale at the matter radiation equality time. The large scale amplitude is almost the same.

proportional to $l_H^{\frac{1}{2}}$. Hence the shift of damping tail location is not so large as that of peak locations. It means also that the width between the sound horizon scale and the diffusion cut off scale becomes thinner.

Next, let us proceed to the variation of fluctuation amplitude which arises from several effects. On the largest angular scale, the amplitude deviates by ω_0^{-1} as in the matter power spectrum. The deviation on a Sachs-Wolfe scale is determined by the value of $\omega(\phi)^{-1}$ at its horizon entry. In fact, the large scale tail in Fig.23 deviates not so large as that in Fig.24 which represents the value of $\omega(\phi)^{-1}$ just at the decoupling time. Moreover, the scalar induced ISW effect is not negligible on large scales. We

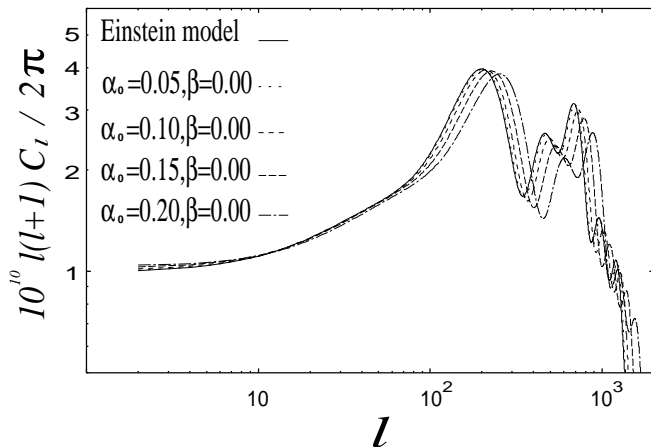


FIG. 21: The COBE normalized CMB temperature anisotropy spectra in the Brans-Dicke models with SCDM parameters.

can see in Fig.25 that it damps the fluctuation amplitude on the scales which are red shifted at the decoupling time. The smaller sound horizon scale at the decoupling time also causes the attenuation of large scale amplitude in l space. As just previously noted, the amplitude on COBE normalization scales is almost model independent. Probably the contributions of several effects cancel each other and the amplitude deviation around these scales is constricted. The foot before the first Doppler peak swells relatively to that in the Einstein model. The scalar induced decay contributes to this enhancement uplifting the originally blue shifted fluctuation, which can also be seen in Fig.25. This decay boosts the acoustic peaks and the first peak is enhanced. Due to the peak location shift, each small scale peak enters the diffusion envelope more deeply than the corresponding peak in the Einstein model and thus it is damped more effectively. As an aside, comparing Fig. 2 and Fig. 23, we expect that the difference between the gravitational constant at the decoupling $G(z = 1000)$ and at the present time G_0 may be constrained as $|G(z = 1000) - G_0|/G_0 < 0.2$. The detailed discussion of observational constraints of the model parameters is our future work.

In the precedent study devoted to the CMB anisotropy in Brans-Dicke cosmology [20], the Brans-Dicke models have higher acoustic peaks. On the contrary, according to our analysis, the Brans-Dicke models have generally lower acoustic peaks. In Fig.22 although the first peak height of the monopole component is almost the same as that in the Einstein model, the attenuation of the dipole component on that angular scale reduces the total peak amplitude.

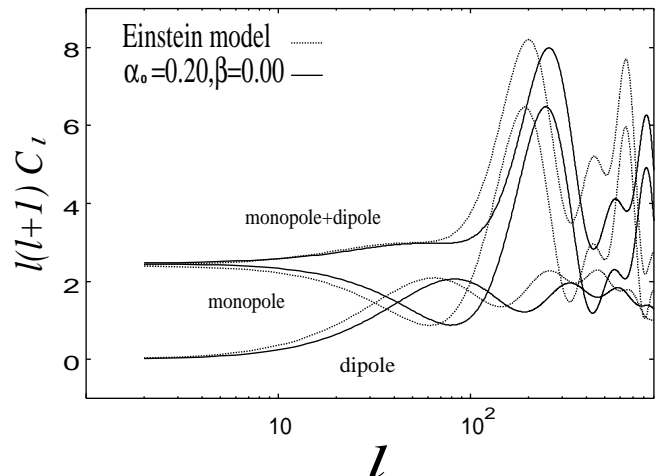


FIG. 22: The component decomposition of the CMB temperature anisotropy spectra in the Einstein and the Brans-Dicke model which is calculated by directly projecting the inhomogeneity spectra at the decoupling time into l space. Normalization is arbitrary. Their curvature perturbations are initially normalized to be the same.

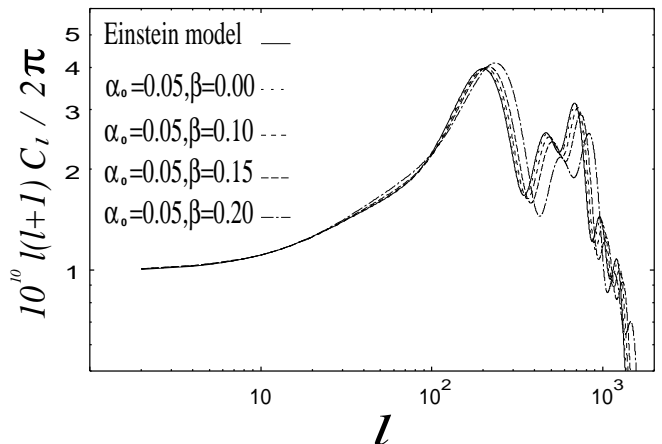


FIG. 23: The COBE normalized CMB temperature anisotropy spectra in the attractor models with SCDM parameters.

VI. CONCLUSION

We have comprehensively studied the perturbation evolution in the scalar-tensor cosmological model. It is shown that the scalar-tensor gravity requires some modification to the standard evolution that is mainly caused by the variable gravitational constant and also brings additional process derived from its fluctuation. We provide the insight into their influence on matter evolution and thus it becomes possible to interpret the variation in the observable quantities.

In the radiation-dominated epoch, the scalar-tensor

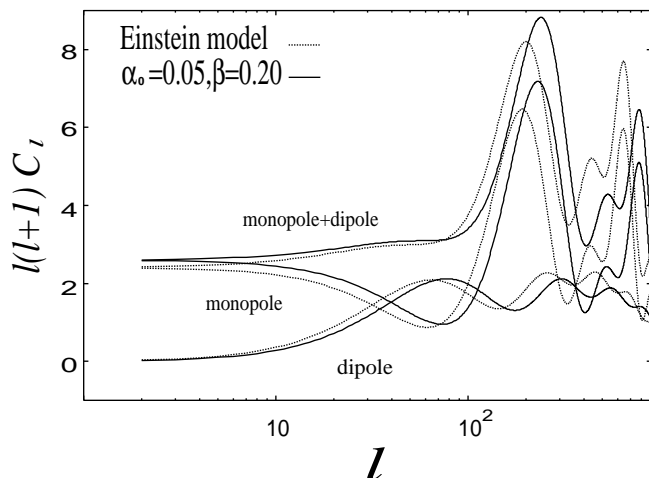


FIG. 24: The component decomposition of the CMB temperature anisotropy spectra in the Einstein and the attractor model which is calculated by directly projecting the inhomogeneity spectra at the decoupling time into l space. Normalization is arbitrary. Their curvature perturbations are initially normalized to be the same.

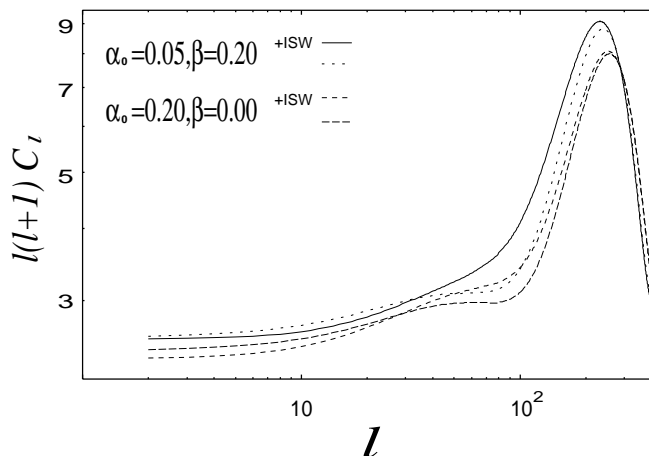


FIG. 25: The contribution of the scalar induced ISW effect to the CMB anisotropy spectra. The spectra not including the ISW contribution are calculated in the same way as in Fig.22 and Fig.24 and then the ISW contribution is added to them. The early ISW effect which is caused by radiation pressure is not included in any curve.

gravity behaves like Einstein gravity. The influence on the perturbation spectrum is the larger horizon length alone. Its observational consequence is the smaller turnover scale in the matter power spectrum. On the other hand, in the matter-dominated epoch, the nature of gravity is qualitatively different from Einstein gravity. Consequently, aside from the shift of the acoustic peak locations and the diffusion cut off scale, the enhancement and the attenuation which originate from the scalar field

perturbation and others appear in the CMB anisotropy spectrum. The attracting scalar-tensor gravity especially affects only the small scale power because of its attracting nature and the degree is far beyond the post-Newtonian deviation at the present epoch.

In this paper, we have concentrated on studying the influence of the scalar-tensor gravity to cosmological perturbations and their resultant observable power spectra. In the future work, we will put constraint on the model parameters α_0 and β by using the precise CMB and large scale structure data provided in near future.

Acknowledgments

T.C. was supported in part by a Grant-in-Aid for Scientific Research (No.13740154) from the Japan Society for the Promotion of Science and by a Grant-in-Aid for Scientific Research on Priority Areas (No.14047212) from the Ministry of Education, Science, Sports and Culture, Japan. N.S. is supported by the Alexander von Humboldt Foundation and a Japanese Grant-in-Aid for Science Research Fund of the Ministry of Education, No. 14540290.

APPENDIX: ANALYTIC APPROACH

In this Appendix, the analytic approximate solutions of both the background and the perturbation equations in Brans-Dicke cosmology are presented (hence ω is constant here). Although these solutions are applicable only to Brans-Dicke models, we can use them for interpreting our numerical results of the variable ω models. The background cosmology is a flat SCDM model. To derive the approximate solutions, we expand the solutions perturbatively by ω^{-1} . To the 0th order in ω^{-1} , we regard ϕ as constant, $\phi = 1$. (Therefore, X_c is vanished to the 0th order in ω^{-1} .) This means we fix the homogeneous solution of Eq.(12) to the 0th order in ω^{-1} . Hence the 0th order equations and their solutions are the same as those in the Einstein model. The purpose of this section is to derive the corrections linear order in ω^{-1} . Higher order corrections are neglected here. (Hence this treatment is applicable only in large ω models)

1. Background

Several authors have studied cosmological solutions in Brans-Dicke cosmology [18]-[25]. Here, we show the cosmological solution which is valid from the radiation-dominated epoch to the matter-dominated epoch. In the background cosmology, the linear order in ω^{-1} is assigned to ϕ' , because the 0th order of ϕ is constant and the force term of Eq.(12) is the linear order in ω^{-1} . Since Eq.(12) is the linear order in ω^{-1} , we can substitute 0th order solutions to the coefficient of each term and obtain the

linear order correction of the constant 0th order solution of ϕ . In both the radiation-dominated epoch and the matter-dominated epoch, the homogeneous solution of Eq.(12) consists of $\phi' = 0$, which corresponds to another choice of G in Einstein gravity, and a decaying mode. More generally, we must give the boundary conditions for Hubble parameter and matter energy density to fix the magnitude of the decaying mode. However, we assume that the decaying mode is already negligible at $z \sim 10^8$ (the initial time of our numerical calculations), otherwise it significantly affects the thermal history in the earlier epochs. (If the homogeneous decaying mode is dominant in ϕ' , the energy density of ϕ is proportional to a^{-6} . It is stiffer than that of radiation fluid.) So we employ, as the main contribution to the solution of Eq.(12), its particular solution that is

$$\phi' = \frac{\sqrt{2} H_{eq} a_{eq}^3}{\omega a^2} \left(1 - \left(1 + \frac{a}{a_{eq}} \right)^{\frac{1}{2}} \left(1 - \frac{a}{2a_{eq}} \right) \right), \quad (\text{A.1})$$

where a_{eq} and H_{eq} are the scale factor and Hubble parameter without $O(\omega^{-1})$ corrections at the matter-radiation equality time. Specifically, this choice determines the deviation of Ω_0 from unity. Integrating the above equation, we obtain

$$\phi = \phi_0 + f(a) - f(a_0), \quad (\text{A.2})$$

where

$$f(a) = \frac{2}{\omega} \left[\frac{a_{eq}}{a} - \frac{a_{eq}}{a} \left(1 + \frac{a}{a_{eq}} \right)^{\frac{1}{2}} + \frac{1}{2} \ln \left\{ \frac{a}{a_{eq}} \cdot \frac{\left(1 + \frac{a}{a_{eq}} \right)^{\frac{1}{2}} + 1}{\left(1 + \frac{a}{a_{eq}} \right)^{\frac{1}{2}} - 1} \right\} \right], \quad (\text{A.3})$$

and a_0 is the present scale factor. The boundary value ϕ_0 is $1 + \frac{1}{2\omega} + O(\omega^{-2})$.

a. Radiation-dominated epoch

In the radiation-dominated epoch, Eq.(A.3) is reduced to

$$f(a) = \frac{1}{\omega} \left(\ln 4 - 1 + \frac{3}{4} \frac{a}{a_{eq}} \right). \quad (\text{A.4})$$

We neglect $O(a^2/a_{eq}^2)$ corrections here. In the period that $a/a_{eq} \ll 1$ is valid (i.e. early times in the radiation-dominated epoch), the last term can be neglected. This behavior of ϕ is well known [18]. The contributions of ϕ' and time variation of ϕ to a'/a are still smaller order than that of CDM energy density. This is because ϕ is driven via the nonminimal coupling whose amplitude is regulated by the energy density of non relativistic matter. Then, we obtain the same relation between η and the expansion rate as that in Einstein gravity,

$$\eta = \left(\frac{a'}{a} \right)^{-1}. \quad (\text{A.5})$$

b. Matter-dominated epoch

The solution in the matter-dominated epoch is,

$$f(a) = \frac{1}{\omega} \ln(a/a_{eq}). \quad (\text{A.6})$$

So Eq.(A.2) becomes

$$\phi = \phi_0 + \frac{1}{\omega} \ln(a/a_0). \quad (\text{A.7})$$

The widely known power-law solution

$$\phi = \phi_0 \left(\frac{a}{a_0} \right)^{\frac{1}{\omega+1}} \quad (\text{A.8})$$

is reduced to Eq.(A.7) with $O(\omega^{-2})$ corrections. Using the Eq.(A.7), we obtain the following relation,

$$\eta = 2 \left(1 - \frac{1}{\omega} \right) \left(\frac{a'}{a} \right)^{-1}. \quad (\text{A.9})$$

2. Perturbation

In this section, introducing a new parameter

$$x \equiv k\eta, \quad (\text{A.10})$$

we derive the solutions of the perturbation equations. Obviously x is smaller than unity on superhorizon scales and larger on subhorizon scales. C_r and C_m in the following sections are proportionality constants.

a. Radiation-dominated epoch

We consider only the adiabatic initial conditions for matter perturbations in which $\Gamma = 0$. Here we also drop the anisotropic pressure correction to simplify the problem. The 0th order initial conditions for matter perturbations are the same as those in Einstein gravity. Employing the parameter x and neglecting the subdominant terms, Eq.(59) is reduced to

$$\frac{d^2}{dx^2} X_c + \frac{2}{x} \frac{d}{dx} X_c + X_c = \frac{3}{8\omega x} \frac{a}{a_{eq}} \left(\frac{d}{dx} \Delta_c + \frac{1}{x} \Delta_c \right) \quad (\text{A.11})$$

in the radiation-dominated epoch. The 0th order solution of Δ_c is

$$\Delta_c^{(0)}/C_r = \left(\frac{9\sqrt{3}}{x} \sin(x/\sqrt{3}) - 9 \cos(x/\sqrt{3}) \right). \quad (\text{A.12})$$

Then, as in the background case, we employ only the particular solution of Eq.(A.11) which is

$$X_c/C_r = \frac{27\sqrt{3}}{16\omega x} \frac{a}{a_{eq}} \left\{ \sin(x/\sqrt{3}) + \frac{\sqrt{3}}{x} \left(\cos x - \cos(x/\sqrt{3}) \right) \right\}. \quad (\text{A.13})$$

(The particular solution is the only growing mode in X_c . If the homogeneous mode exists in X_c , it forms the gravitational potential perturbation decreasing with time.) The behavior of this solution is as follows

$$X_c/C_r = \begin{cases} \frac{3}{32\omega}(a/a_{eq})x^2 & \text{Superhorizon} \\ \frac{27}{16\omega}(a/a_{eq})\frac{\sin(x/\sqrt{3})}{(x/\sqrt{3})} & \text{Subhorizon} \end{cases} \quad (\text{A.14})$$

Before the horizon entry, driven by the nonminimal coupling, X_c grows proportional to x^2 . After the horizon entry, it stops growing and begins to oscillate. The first term in the parenthesis in Eq.(A.13) ($\cos x$) whose frequency is different from other terms represents the propagation of ϕ fluctuation and damps as the universe expands. The oscillation of the remaining terms is driven by the matter acoustic oscillation which affects X_c via metric perturbations. The factor $1/\sqrt{3}$ in their argument represents the radiation sound velocity. It is clear that the contribution of the additional terms in Eq.(58) and (60) to the gravitational potential is at most order $(a/a_{eq})\omega^{-1}$ which is still smaller order than that of CDM perturbation. Hence, at the initial time early enough, the initial conditions for matter perturbations are not modified. The relevant numerical solution is illustrated in Fig.6.

b. Matter-dominated epoch

In the matter-dominated epoch, the terms associated with c_s^2 or w are neglected, and then Eq.(59) is reduced to

$$\frac{d^2}{dx^2}X_c + \frac{4}{x}\frac{d}{dx}X_c + X_c = \frac{2}{\omega x}\frac{d}{dx}\Delta_c + \frac{6}{\omega x^2}\Delta_c. \quad (\text{A.15})$$

The modified evolution equation for Δ_c becomes

$$\begin{aligned} \frac{d^2}{dx^2}\Delta_c + \frac{2}{x}\frac{d}{dx}\Delta_c - \frac{6}{x^2}\Delta_c &= \frac{2}{\omega x}\frac{d}{dx}\Delta_c \\ -\frac{4}{\omega x^2}\Delta_c + \frac{d^2}{dx^2}X_c + \frac{2}{x}\frac{d}{dx}X_c - \frac{6}{x^2}X_c &. \end{aligned} \quad (\text{A.16})$$

Here we use Eq.(A.15). Obviously the homogeneous growing mode solution (the 0th order in ω^{-1}) of Eq.(A.16) is proportional to x^2 . Let C_m be the proportionality constant of it. Then, the particular solution of Eq.(A.15) is

$$X_c/C_m = \frac{10}{\omega}\left(1 - \frac{3\sin x}{x^3} + \frac{3\cos x}{x^2}\right). \quad (\text{A.17})$$

The asymptotic forms are

$$X_c/C_m = \begin{cases} \frac{1}{\omega}x^2 & \text{Superhorizon} \\ \frac{10}{\omega} & \text{Subhorizon} \end{cases} \quad (\text{A.18})$$

Before the horizon entry, it grows as in the radiation-dominated epoch. After the horizon entry, the propagation mode damps away and the constant mode supported by the nonminimal coupling remains. The constancy of the surviving term is due to the constancy of the gravitational potential. This convergence of X_c is illustrated in Fig.7. Substituting Eq.(A.17) into Eq.(A.16), we obtain the modified solution of Δ_c as follows

$$\Delta_c/C_m = x^2 + \frac{1}{\omega}\left\{30\left(\frac{\cos x}{x^2} - \frac{\sin x}{x^3}\right) + 10 - x^2\right\}. \quad (\text{A.19})$$

The asymptotic forms of the correction terms are

$$\Delta_c^{(1)}/C_m = \begin{cases} -\frac{1}{840\omega}x^4 & \text{Superhorizon} \\ -\frac{1}{\omega}x^2 & \text{Subhorizon} \end{cases} \quad (\text{A.20})$$

This correction is negligible until the horizon entry, and after the horizon entry the amplitude of the density perturbation is slightly suppressed. Then, the solution of the gravitational potential with $O(\omega^{-1})$ accuracy becomes

$$(\Phi_s - \Psi_s)/C_m = 12 + \frac{1}{\omega}\left\{60\left(\frac{3\sin x}{x^5} - \frac{3\cos x}{x^4} - \frac{\sin x}{x^3}\right) - 26\right\}. \quad (\text{A.21})$$

At the horizon crossing, transient decay is induced by the suppression of X_c growth. However, before and after the crossing time, the linear order correction of the gravitational potential is flat as in the case of the 0th order.

$$(\Phi_s - \Psi_s)^{(1)}/C_m = \begin{cases} -\frac{22}{\omega} & \text{Superhorizon} \\ -\frac{26}{\omega} & \text{Subhorizon} \end{cases} \quad (\text{A.22})$$

Finally, we mention the proportionality constants. Comparing the same scale modes in the two models ever since the radiation-dominated epoch, we obtain the different C_m s even if initially we set the C_r s to the same value. C_m itself contains the $O(\omega^{-1})$ correction which represents the deviation formed around the matter-radiation equality time. On superhorizon scales, the correction coefficient of the proportionality constant is

$$C_m^{BD}/C_m^E \simeq 1 + \frac{19}{10\omega} \quad (\text{A.23})$$

according to our numerical calculations.

[1] M. B. Green, J. H. Schwarz, and E. Witten, *Superstring Theory* (Cambridge University Press, Cambridge, Eng-

land, 1987).

- [2] J. K. Webb, M. T. Murphy, V. V. Flambaum, V. A. Dzuba, J. D. Barrow, C. W. Churchill, J. X. Prochaska, and A. M. Wolfe, *Phys. Rev. Lett.* **87**, 091301 (2001)
- [3] P. Jordan, *Nature (London)* **164**, 637 (1949); *Schwerkraft und Weltall* (Vieweg, Braunschweig, 1955); *Z. Phys.* **157**, 112 (1959).
- [4] C. Brans and R. H. Dicke, *Phys. Rev.* **124**, 925 (1961); R.H.Dicke, *ibid.* **125**, 2163 (1962); **152**, 1 (1968).
- [5] P. G. Bergmann, *Int. J. Theor. Phys.* **1**, 25 (1968); R. V. Wagoner, *Phys. Rev. D* **1**, 3209 (1970).
- [6] D. La and P. J. Steinhardt, *Phys. Rev. Lett.* **62**, 376 (1989); *Phys. Lett. B* **220**, 375 (1989).
- [7] E. J. Weinberg, *Phys. Rev. D* **40**, 3950 (1989); D. La, P. J. Steinhardt, and E. W. Bertschinger, *Phys. Lett. B* **231**, 231 (1989).
- [8] P. J. Steinhardt and F. S. Accetta, *Phys. Rev. Lett.* **64**, 2740 (1990); J. D. Barrow and K. Maeda, *Nucl. Phys.* **B341**, 1990 (1990); J. Garcia-Bellido and M. Quiros, *Phys. Lett. B* **243**, 45 (1990); R. Holman, E. W. Kolb, and Y. Wang, *Phys. Rev. Lett.* **65**, 17 (1990).
- [9] A. D. Linde, *Phys. Lett. B* **238**, 160 (1990).
- [10] T. Chiba, arXiv:gr-qc/0110118; J. P. Uzan, hep-ph/0205340.
- [11] R. D. Reasenberg *et al.*, *Astrophys. J.* **234**, L219 (1979).
- [12] C. M. Will, *Theory and Experiment in Gravitational Physics* (Cambridge University Press, Cambridge, England, 1981).
- [13] C. M. Will, gr-qc/0103036.
- [14] T. Damour and K. Nordtvedt, *Phys. Rev. Lett.* **70**, 2217 (1993); *Phys. Rev. D* **48**, 3436 (1993).
- [15] T. Damour and B. Pichon, *Phys. Rev. D* **59**, 123502 (1999).
- [16] MAP: <http://map.gsfc.nasa.gov>.
- [17] Planck: <http://astro.estec.esa.nl/Planck>.
- [18] H. Nariai, *Prog. Theor. Phys.* **42**, 544 (1969).
- [19] A. R. Liddle, A. Mazumdar and J. D. Barrow, *Phys. Rev. D* **58**, 027302 (1998).
- [20] X. Chen and M. Kamionkowski, *Phys. Rev. D* **60**, 104036 (1999).
- [21] J. M. Bardeen, *Phys. Rev. D* **22**, 1882 (1980).
- [22] H. Kodama and M. Sasaki, *Prog. Theor. Phys. Supp.* **78**, 1 (1984).
- [23] L. E. Gurevich, A. M. Finkelstein, and V. A. Ruban, *Astrophys. Space Sci.* **22**, 231 (1973).
- [24] J. D. Barrow and P. Parsons, *Phys. Rev. D* **55**, 1906 (1997).
- [25] D. J. Holden and D. Wands, *Class. Quantum Grav.* **15**, 3271 (1998).